Available online at www.sciencedirect.com
SCIENCE DIRECT
Journal of Sound and Vibration 294 (2006) 841–855
JOURNAL OF SOUND AND VIBRATION
www.elsevier.com/locate/jsvi

Application of analytic wavelet transform to analysis of highly impulsive noises

Xiangdong Zhu, Jay Kim*

Structural Dynamics Research Laboratories, Mechanical Engineering Department, University of Cincinnati, Cincinnati, OH 45221-0072, USA

Received 9 February 2005; received in revised form 14 November 2005; accepted 12 December 2005
Available online 28 February 2006

Abstract

Time–frequency (*T–F*) domain analysis is necessary to characterize highly transient signals. The analytic wavelet transform (AWT), which has features of both the Fourier transform and the wavelet transform, is advocated as an ideal *T–F* signal analysis tool in this paper. Underlying theories and basic properties of the AWT are discussed in comparison with a commonly used short-time Fourier transform (STFT) method. The AWT is set up specifically for acoustics applications to describe *T–F* changes of the signal in sound pressure level, and applied to characterize two highly impulsive sound signals. Comparing the results from the AWT and the STFT clearly demonstrates the advantage of the AWT, which captures temporal and spectral characteristics of the signal in much more detail. A potential application of the AWT to risk assessment of impulsive noise-induced hearing loss is discussed.

1. Introduction

Characteristics of a transient signal should be described in the joint time–frequency (*T–F*) domain because of spectral characteristics of the signal change with respect to time. The time history or the frequency spectrum alone is not sufficient to understand transient signals. For example in music, the quantities which we perceive as the "amplitude" and "frequency" both change as functions of time. In fact, time and frequency are not separate but interwoven concepts in transient events [1]. Impulsive noises that arise in industrial or military environments are also examples. The difficulty in assessing the risk of impulsive noises to human hearing loss has been one of the major concerns of occupational health research [2], which may be partially attributed to the lack of easily available, efficient *T–F* signal analysis methods.

The short-time Fourier transform (STFT) has been widely used for transient signal analysis, which is a straightforward extension of the Fourier transform. The method essentially involves applying the Fourier transform repeatedly, each time moving the time window [3]. A three-dimensional (3-D) representation of the result of STFT is called water-fall plot, which many commercial signal analysis programs provide as a default option. While its application is easy since the method is based on the Fourier transform, the STFT is a poor

*Corresponding author.
E-mail address: Jay.kim@uc.edu (J. Kim).

0022-460X/$ - see front matter © 2006 Elsevier Ltd. All rights reserved.
doi:10.1016/j.jsv.2005.12.034

choice for highly transient signals. Heisenberg's principle [1] states that the spectral and temporal resolutions of the T–F signal representation cannot be improved simultaneously. The STFT uses a single T–F atom in the entire T–F domain [3]; therefore lacks the temporal resolution for high frequency (temporally fast) components and lacks the spectral resolution for low frequency (temporally slow) components. In other words, the STFT result always suffers from the lack of either temporal or spectral resolution [1,3].

The wavelet transform, a relatively new signal analysis method introduced in the 1970s [4,5], decomposes signals using wavelets of variable scales, which are obtained by dilating and scaling the mother wavelet. The main advantage of the wavelet transform stems from the fact that it uses variable scales, therefore variable T–F resolutions. The transform with a small-scale wavelet uses a T–F atom short in time and wide in frequency, thus picks up fast changing components efficiently, while the transform with a large-scale wavelet uses a T–F atom long in time and narrow in frequency, thus picks up slowly changing components efficiently.

The wavelet analysis has found a broad range of applications such as signal compression, fault detection, edge detection, and de-noising of signals [1]. However, it is interesting that the method has seldom been applied to the quantitative analysis of transient signals, seemingly the most straightforward and natural application of the method. This may have been caused by a reluctance of end-users due to the need to learn new theories and concepts. As it will be shown in this paper, the analytic wavelet transform (AWT) provides a perfect solution for this situation. At first, the information obtained from the AWT can be represented and interpreted in exactly the same way as in the STFT. Secondly, the AWT process can be made numerically nearly as efficient as the STFT if it is programmed properly. With the AWT setup in the way used in this paper, end-users will not even notice the difference in using the AWT from using the STFT; the AWT just provides much clearer information on T–F characteristics of the signal. It seems there simply is no reason not to use the AWT over the STFT for transient signal analysis.

2. Brief theory of AWT

2.1. Analytic function

An analytic function $f_a(t)$ is a complex function whose Fourier transform has no components in the negative frequency range [1]. The Fourier transform of its real part, $f = \mathrm{Re}[f_a]$, is

$$\hat{f}(\omega) = \frac{\hat{f}_a(\omega) + f_a^*(-\omega)}{2}, \tag{1}$$

where $\hat{f}(\omega)$ stands for the Fourier transform of $f(t)$, * stands for the complex conjugate and Re stands for the real part. This relation can be inverted to

$$\hat{f}_a(\omega) = \begin{cases} 2\hat{f}(\omega) & \text{if} \quad \omega \geqslant 0, \\ 0 & \text{if} \quad \omega < 0. \end{cases} \tag{2}$$

Therefore, the analytic part $f_a(t)$ of the signal $f(t)$ is the inverse Fourier transform of $\hat{f}_a(\omega)$ defined in Eq. (2).

2.2. Analytic wavelet transform

The mother wavelet of the AWT is defined as

$$\psi(t) = g(t)\mathrm{e}^{\mathrm{j}\eta t}, \tag{3}$$

where $\mathrm{j} = \sqrt{-1}$, η is a parameter that will be related to the frequency, and $g(t)$ is a real-valued function such that $g(t) \to 0 \quad \text{as} \quad |t| \to \infty$. A Gaussian function is a popular choice for $g(t)$, which is used in this work

$$g(t) = \frac{1}{(\sigma^2\pi)^{1/4}}\mathrm{e}^{-t^2/2\sigma^2}. \tag{4}$$

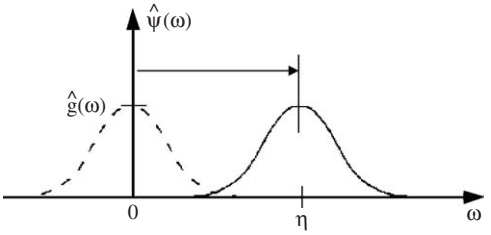

Fig. 1. Mother wavelet of the Morlet wavelet.

In Eq. (4), parameter σ determines the shape of the function. The complex wavelet defined by Eqs. (3) and (4) is called the Morlet wavelet [1].

The Fourier transforms of $g(t)$ and $\psi(t)$ are given as

$$\hat{g}(\omega) = (4\pi\sigma^2)^{1/4} e^{-\sigma^2\omega^2/2}, \quad \hat{\psi}(\omega) = \hat{g}(\omega - \eta). \tag{5,6}$$

Fig. 1 illustrates $\hat{\psi}(\omega)$ in relation to η, which is obtained by shifting $\hat{g}(\omega)$ by η to right. From Fig. 1, it is known that the one-sided condition in Eq. (2) that an analytic function should satisfy will be satisfied approximately if $\sigma^2\eta^2 \gg 1$ because $\hat{g}(\omega - \eta) \approx 0$ for $\omega < 0$. Because $\hat{\psi}(0) \cong 0$, the AWT also removes the contribution of the DC component of the signal [6].

With the mother wavelet defined in Eq. (4), the AWT is defined as any other continuous wavelet transform as follows:

$$W_s(u) = \langle f(t), \psi_{u,s} \rangle = \int_{-\infty}^{\infty} f(t)\, \psi_{u,s}^*\, dt, \tag{7}$$

where $\langle f, \psi_{u,s} \rangle$ stands for the scalar product. The family of wavelets $\psi_{u,s}$ is obtained by dilating and translating the mother wavelet ψ:

$$\psi_{u,s}(t) = \frac{1}{s}\psi\left(\frac{t-u}{s}\right), \tag{8}$$

where s is the scale and u is the translation amount.

The wavelet defined in Eq. (8) has a constant area norm because

$$\|\psi_{u,s}(t)\| = \int_{-\infty}^{\infty} \psi_{u,s}(t)\, dt = \int_{-\infty}^{\infty} \frac{1}{s}\psi\left(\frac{t-u}{s}\right) dt = \|\psi(t)\| = \text{constant}. \tag{9}$$

Slightly different definitions can also be used. For example, wavelets defined as $\psi_{u,s}(t) = (1/\sqrt{s})\psi(t - u/s)$ will have a constant square norm. The AWT using the wavelet defined in Eq. (8) becomes similar to the Fourier transform with a moving time window of variable window size.

2.3. Comparison of AWT to Fourier transform

The wavelet transform defined in Eq. (7) can be rewritten as

$$W_s(u) = \int_{-\infty}^{\infty} f(t)\, \psi_{u,s}^*(t)\, dt = \int_{-\infty}^{\infty} \frac{1}{s} f(t)\, g\left(\frac{t-u}{s}\right) e^{-j\eta(t-u/s)}\, dt. \tag{10}$$

If we let $t^* = t - u$, Eq. (10) becomes

$$W_s(u) = \int_{-\infty}^{\infty} f(t^* + u)\, \frac{1}{s} g\left(\frac{t^*}{s}\right) e^{-j(\eta/s)t^*}\, dt^*. \tag{11}$$

The integration defined in Eq. (11) can be interpreted graphically as in Fig. 2. The illustration shows that the AWT can be understood as a Fourier transform with a time window $(1/s)g(t/s)$ located at $t = u$. Comparing

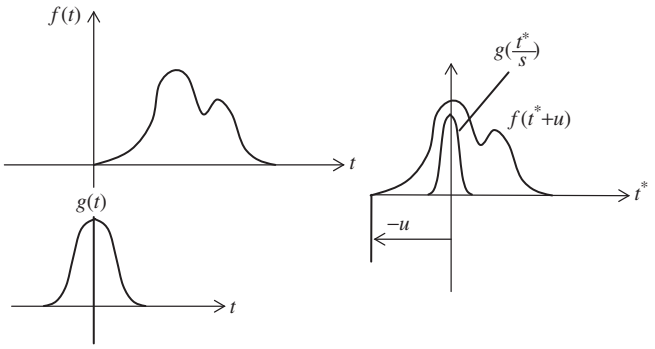

Fig. 2. Graphical interpretation of analytic wavelet transform.

the AWT defined in Eq. (11) with the Fourier transform equation, it is recognized that

$$\omega = \frac{\eta}{s}. \tag{12}$$

Therefore, the result of the AWT defined in Eq. (11) with given s and u is the frequency component of the signal corresponding to $\omega = \eta/s$ at the instant $t = u$. The magnitude and argument of the component represent the amplitude and phase of the component as in the Fourier transform. Repeating the integration over the entire range of u finds the time history of the frequency component, which is actually done by a single convolution integral (see Eq. (13)). The complete *T–F* description of the signal is obtained by conducting this convolution integral over the range of scale that covers all the frequency of interest. Choice of $g(t)$ determines $\hat{g}(\omega)$, thus determines the shape of the frequency filter of the AWT.

2.4. Numerical implementation of AWT

Because the Gaussian function used for $g(t)$ is a symmetric function, Eq. (10) can be written in a convolution integral form

$$W_s(u) = \int_{-\infty}^{\infty} f(t)\ \frac{1}{s} g\left(\frac{u-t}{s}\right) e^{j\eta(u-t/s)}\, dt = \mathrm{conv}(f(t), h_s(t)), \tag{13}$$

where

$$h_s(t) = \frac{1}{s} g(t/s) e^{j\eta(t/s)}. \tag{14}$$

Evaluation of the convolution integral defined in Eq. (13) for a given s results in the time series that represents the signal components contained in the frequency range determined by $\hat{g}(\omega)$ centered at $\omega = \eta/s$.

The wavelet transform defined in Eq. (13) can be evaluated in a computationally efficient way by using the convolution theorem in the frequency domain as follows:

$$\mathrm{F}(W_s(u)) = \hat{W}_s(\omega) = \hat{f}(\omega)\hat{h}_s(\omega), \tag{15}$$

where $\hat{f}(\omega)$ and $\hat{h}(\omega)$ are the Fourier transforms of $f(t)$ and $h(t)$. Therefore, the AWT result can be obtained by the inverse Fourier transform of $\hat{W}_s(\omega)$:

$$W_s(u) = \mathrm{F}^{-1}(\hat{f}(\omega)\, \hat{h}_s(\omega)), \tag{16}$$

where F^{-1} stands for the inverse Fourier transform. One can show that

$$\hat{h}_s(\omega) = \int_{-\infty}^{\infty} \frac{1}{s}\ g(t/s) e^{j\eta(t/s)} e^{-j\omega t}\, dt = \hat{g}(\eta - s\omega). \tag{17}$$

In the entire operation, $\hat{g}(\omega)$ has to be estimated only once. Then, $\hat{h}_s(\omega)$ is found by simply substituting $\eta - s\omega$ into $\hat{g}(\omega)$. Fourier transform is necessary only once in the entire AWT operation when $\hat{f}(\omega)$ is obtained. At each scale of AWT operation, $\hat{f}(\omega)$ and $\hat{g}(s\omega - \eta)$ should be multiplied, thus a multiplication of two vectors is required, and one inverse Fourier transform is required to be performed for $\mathrm{F}^{-1}(\hat{f}(\omega)\,\hat{h}_s(\omega))$. A comparable STFT requires as many Fourier transforms as the number of time points to make the T–F plot. Actual computational demands for the AWT and STFT vary depending on the number of scales and time points used for the AWT and STFT; however, they are quite comparable, and certainly in the same order of magnitude.

2.5. Selection of AWT parameters

As discussed before, the choice of $\hat{h}_s(\omega) = \hat{g}(\eta - s\omega)$ dictates the frequency filter effect of the AWT. Parameters of the Gaussian function $g(t)$ can be chosen for a desired filter effect. In this work, $g(t)$ is set up for a 1/3 octave filter effect. With reference to Fig. 3 and Eq. (5), it is easy to show that

$$\hat{g}(\eta - s\omega) = (4\pi\sigma^2)^{1/4}\,\mathrm{e}^{-\sigma^2(\eta - s\omega)^2/2}. \tag{18}$$

The center, lower limt and upper limt frequencies of the 1/3 octave filter are given as

$$\omega_c = \frac{\eta}{s}, \quad \omega_l = 2^{-1/6}\omega_c, \quad \omega_u = 2^{1/6}\omega_c. \tag{19}$$

The level difference between the center and lower frequencies is

$$\begin{aligned} \Delta dB_l &= 20\log_{10}\frac{g(\eta - s\omega_l)}{g(\eta - s\omega_c)} = 20\log_{10}\frac{g(\eta - s\omega_l)}{g(0)} \\ &= -10\sigma^2\eta^2(1 - 2^{-1/6})^2/\log_{\mathrm{e}} 10. \end{aligned} \tag{20}$$

Similarly the difference between the center frequency and the upper limit frequency is

$$\Delta dB_u = -10\sigma^2\eta^2(1 - 2^{1/6})^2/\log_{\mathrm{e}} 10. \tag{21}$$

To make a 3 dB level drop at the upper and lower limit frequencies, it is known from Eqs. (20) or (21) that η and σ have to be chosen so that $\sigma^2\eta^2 = 58$. Adopting $\sigma = 1$, $\eta = 7.6$ has to be used. With this setup, performing the AWT returns the amplitude of the signal components contained in the frequency range of the 1/3 octave band centered at $\omega_c = \eta/s$.

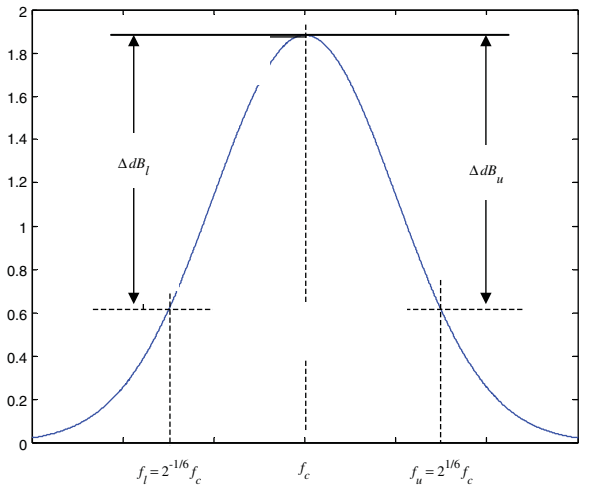

Fig. 3. Shape of the amplitude of wavelet function in the frequency domain.

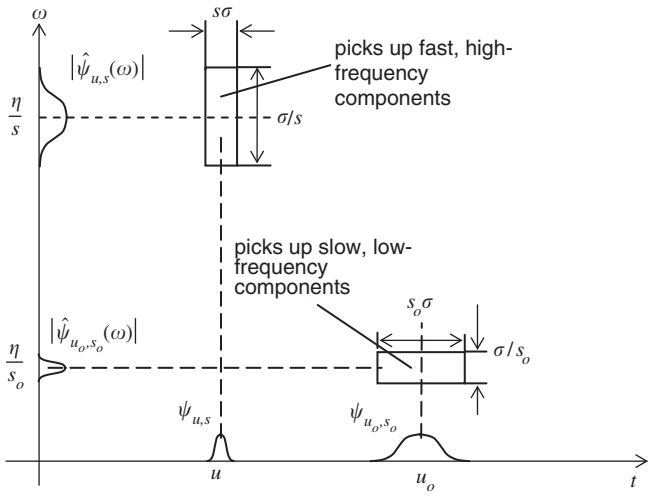

Fig. 4. Time–frequency atom of the wavelet transform.

2.6. Time–frequency atom

According to Eqs. (13), (14) and (16), (17), it is recognized that the time and frequency filter sizes will be proportional to $s\sigma$ and σ/s, respectively, which define the T–F atom of the AWT. T–F atom may be understood as the unit to break down the signal in the T–F domain [1]. The area of the T–F atom is obviously constant, which is essentially the Heisenberg principle: the time and frequency resolutions cannot be improved at the same time [1,3].

The STFT uses a single T–F atom in the entire T–F domain, whose time size is the length of the time window and the frequency size is the inverse of the time window size. Therefore, STFT results always lack temporal resolution for fast signal components and lack spectral resolution for slow signal components. On the other hand, the T–F atom of the AWT is dependent on the scale s as it was discussed. As the scale s decreases, both the center frequency ($\omega_c = \eta/s$) and the frequency size of the T–F atom increase but the time size of the atom decreases, which makes the wavelet transform ideal to pick up fast changing (i.e., high frequency) components of the signal. As the scale s increases, the opposite occurs; the wavelet transform becomes ideal to pick up slow-changing (i.e., low frequency) signal components. This is because the AWT uses variable T–F atoms. The concept is illustrated in Fig. 4 [1].

3. Test cases for AWT

The AWT is applied to two test cases. The test signals are a sine function and a time-domain Dirac delta function. The T–F representations of these signals are known in exact forms.

3.1. A sine signal with a constant frequency

A time domain function $f = 5\sin(40\pi t)$ is considered. Fig. 5(a) show the representation obtained by the AWT, and Fig. 5(b) is a view at the plot in Fig. 5(a) from the frequency side. Obviously, the exact representation of the amplitude of the signal in the T–F domain is a vertical wall with height 5 that runs in parallel with the time-axis and intersects the frequency axis at 20 Hz. The figures show the AWT approximates the exact representations very well; the signal is a dispersed form of the exact representation. The curve in Fig. 5(b) is actually the flipped shape of $\hat{g}_s(\omega)$ located at 20 Hz. Fig. 5(c) shows the real and imaginary parts of the AWT result, which resemble $5\sin(40\pi t)$ and $-5\cos(40\pi t)$, respectively. Fig. 5(d)

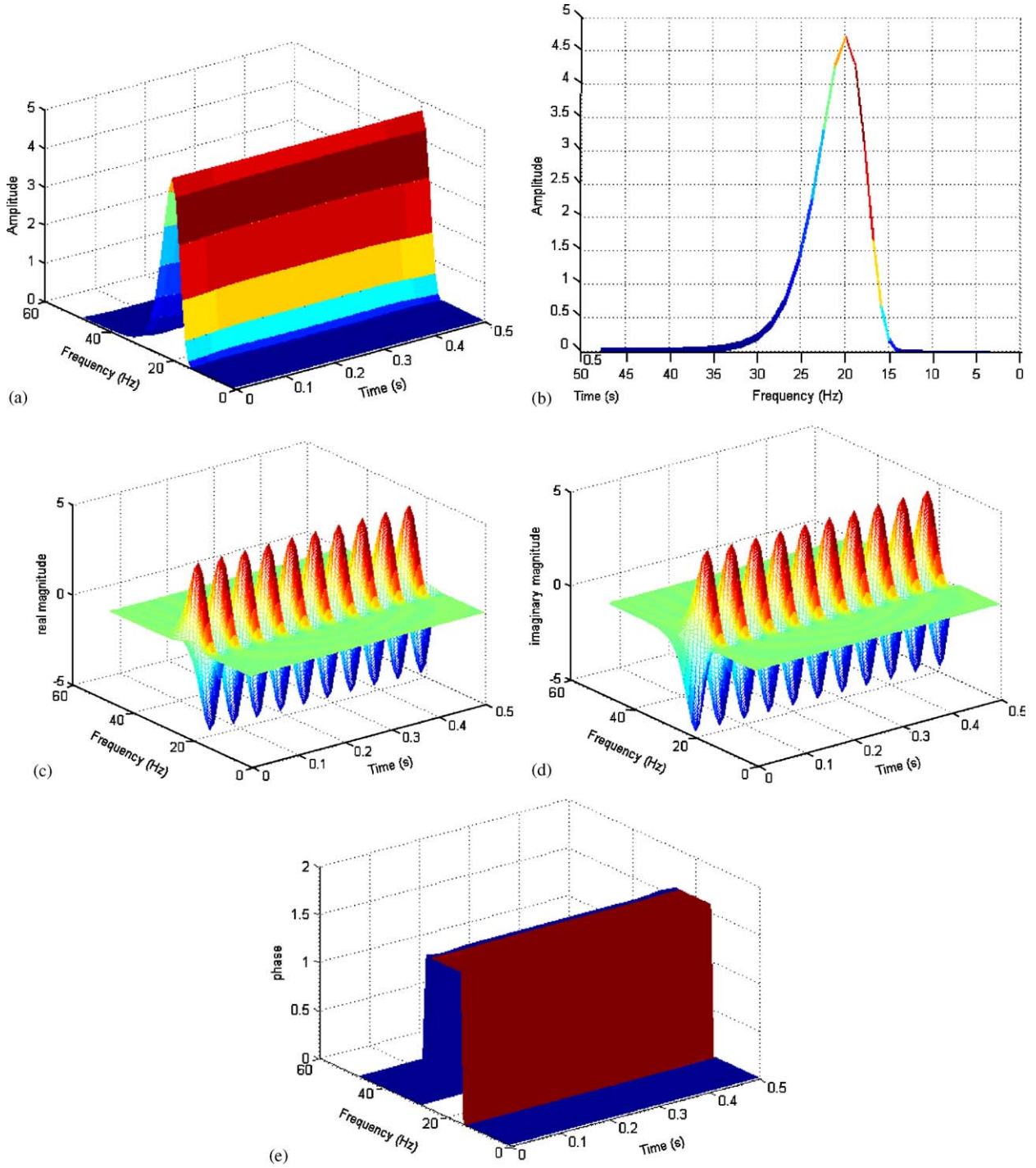

Fig. 5. AWT results of known signals: (a) amplitude of $f = 5\sin(40\pi t)$; (b) amplitude of $f = 5\sin(40\pi t)$, viewed from the frequency side; (c) real part of $f = 5\sin(40\pi t)$; (d) imaginary part of $5\sin(40\pi t)$; and (e) phase plot of $(5\sin 40\pi t - 5\cos 40\pi t)$.

plots the phase difference of $f_1(t) = 5\sin(40\pi t)$ and $f_2(t) = 5\cos(40\pi t)$ captured by the AWT, which is approximately 90° as it should. This shows that the phase information is also calculated correctly the AWT.

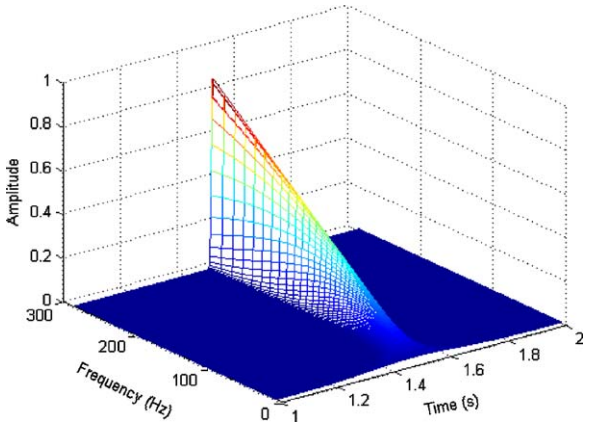

Fig. 6. Amplitude of the signal $f(t) = \delta(t - 1.5)$ captured by the AWT.

3.2. A Dirac delta function

As the next test case, a time-domain Dirac delta function is considered, which is

$$f(t) = 5\,\delta(t - 1.5). \tag{22}$$

Fig. 6 shows the amplitude plot of the signal in the T–F domain obtained by the AWT.

The exact T–F domain representation is a vertical wall located at $t = 1.5$ s whose height increases linearly as the frequency increases. The height increase is due to the use of the 1/3 octave band for the frequency axis, whose band-width increases as the frequency increases. Fig. 6 shows that the AWT result represents the Dirac delta function, an ultimate transient function, very nicely.

4. Application of the AWT to impulse sound signals

Characterization of impulsive noise has been one of major difficulties in the study of noise-induced hearing loss (NIHL), a common occupational disease among industrial workers and military personnel. Current guidelines pertaining to NIHL developed by various organizations such as ISO [7] and the National Institute for Occupational Safety and Health (NIOSH) [8] generally are based on the equal-energy-hypothesis (EEH), a steady-state concept. The practices are based on the premise that the same amount of sound energy will produce the same amount of hearing impairment regardless of how the sound energy is distributed in time [7,9]. However, there is abundant evidence from various clinical and animal model studies, which argue against such a straightforward extension of the EEH to impulsive noise [10–12]. One of the main difficulties in assessing exposure risk to impulsive noise is the quantitative characterization of the noise. An impulse noise is characterized by its peak level, rise and decay times, which are time domain properties. Spectral characteristics of the noise have been considered additionally, but not in any manner related to the temporal characteristics. A highly transient event such as impulsive noise should be characterized in the joint T–F, for which the AWT becomes a perfect solution.

4.1. AWT for sound analysis

As mentioned, the AWT in this work is set up to obtain the complex amplitude that represents the signal components contained in the 1/3 octave band located at $\omega_c = \eta/s$. If the sound pressure signal is in Pa, it can be represented in the sound pressure level (SPL) as

$$\mathrm{SPL}(u)_s = 10\log_{10}\left(\frac{W_s(u)\,W_s(u)^*}{2P_{\mathrm{ref}}^2}\right), \tag{23}$$

where $P_{\mathrm{ref}} = 20 \times 10^{-6}$ Pa. This way, T–F plots can be made in terms of the SPL.

5. Sound from impact power wrench

Fig. 7 shows the time history of the sound generated by an impact power wrench, which was measured at the operator's ear position for a duration of 0.1 s [13]. The sampling rate of 40,000 Hz was used, which corresponds to the Nyquist frequency of 20,000 Hz. Operation of the tool involves very rapid metal-to-metal impacts, which create a train of highly impulsive sounds occurring nearly 50 times per 1 s, each time reaching an instantaneous SPL of nearly 120 dB.

5.1. T–F characterization by STFT

Fig. 8 shows the T–F plot obtained from the STFT of the signal shown in Fig. 7. A time window of 0.02 s size is used for each Fourier transform, which results in the frequency resolution of 50 Hz. About 50% overlapping is used; therefore the window is moved by 0.01 s for each FFT. A-weighting is applied to each spectrum $P(\omega)$ to convert the SPL to dBA.

Since the frequency resolution is $\Delta f = 1/T$, the resolution can be improved by increasing the time window size T, which however decreases the temporal resolution of the T–F data. Using a shorter time window, decreasing T, will improve the temporal resolution; however it will decrease the frequency resolution. In fact,

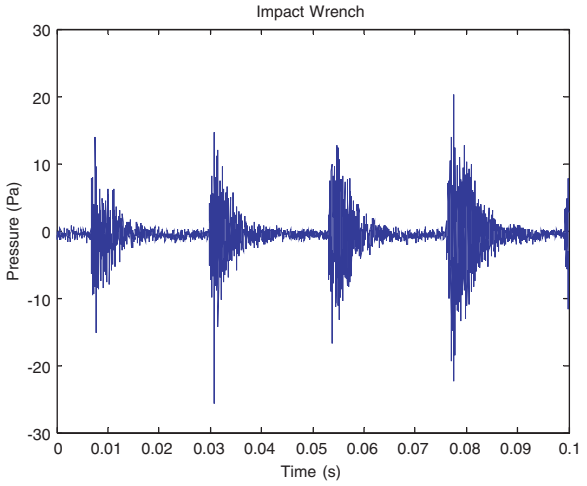

Fig. 7. Time history of the sound from an impact power wrench.

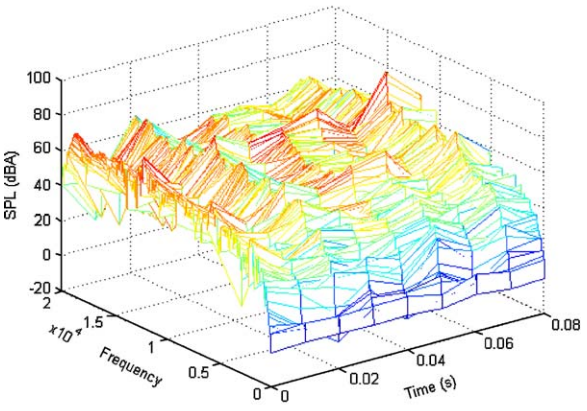

Fig. 8. Time–frequency plot of the SPL of the impact power wrench obtained by STFT.

Fig. 8 was obtained as a best compromise after several trial-and-errors. The limitation of the STFT is obvious from Fig. 8. For example, the maximum SPL of the *T–F* plot is obtained as only 87 dBA at 10,000 Hz, which is significantly lowered by the averaging effect due to the 0.02 s time window, a very long time for such a fast signal.

5.2. *T–F characterization by AWT*

Fig. 9 is the *T–F* plot obtained by applying the AWT to the same signal shown in Fig. 7. The AWT result is converted to the SPL by using Eq. (23), which is then converted to dBA by applying A-weighting. Improvement in the *T–F* resolution from the STFT is remarkable when Fig. 9 is compared with Fig. 8. The highest SPL is now obtained as 105 dB at 8000 Hz 1/3 octave band. Characteristics of the impact noise are well reflected by the relatively flat shape of the surface in the direction of time.

The *T–F* plot in Fig. 9 can be improved by interlacing the frequency plots, which can be done by estimating the AWT at every 1/12 octave points. This provides four intermediate frequency points to the plot in Fig. 9, which makes the surface smoother. The AWT plot obtained as such is shown in Fig. 10. This scheme is used for all subsequent plots.

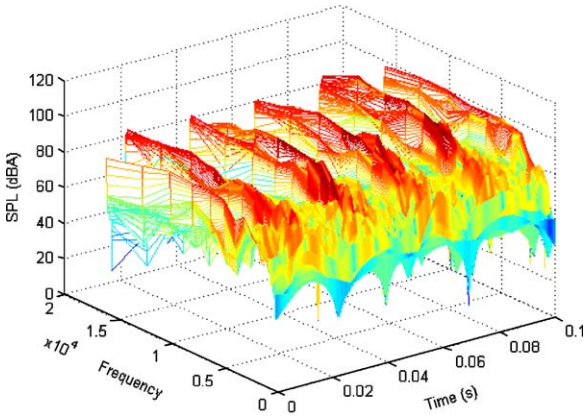

Fig. 9. Time–frequency plot of the SPL of the impact power wrench obtained by AWT.

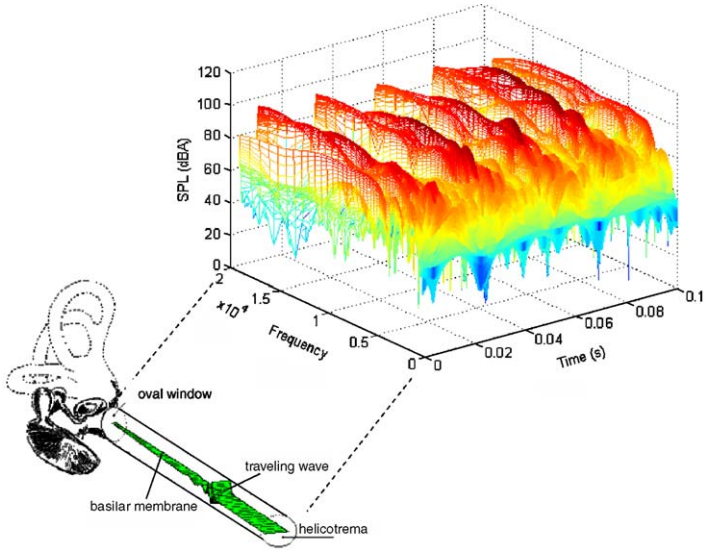

Fig. 10. Time–frequency plot of the SPL of the impact power wrench obtained by AWT using more frequency points.

As illustrated in Fig. 10, the frequency axis of the AWT may be related to the positions of the basilar membrane because 1/3 octave frequencies match with critical bands in a wide range of frequency. Therefore, the curve obtained by cutting the T–F characteristic surface to the time axis direction at a given frequency may be considered as the time history of the stimulus felt by the basilar membrane at the corresponding position. Also, the curve obtained by cutting the surface to the frequency direction at a given time may be interpreted as a snap shot of the basilar membrane displacement. Employing the 1/3 octave band makes use of the effective averaging time of the auditory system as the time constant, thus makes good sense for hearing research purpose. Used this way, the AWT can be very useful for correlation study of the hearing loss and noise characteristics.

5.3. 1/3 octave time histories

The AWT obtained by Eq. (13) is actually the time history of the sound power contained in the 1/3 octave band of center frequency η/s. Fig. 11 shows six 1/3 octave time histories at 0.5, 1, 2, 4, 8 and 16 kHz. It is seen that the time history changes faster at higher frequencies as time atom becomes smaller. These transient 1/3 octave band time histories are new concepts that may have various applications. Six 1/3 octave bands from the STFT are shown in Fig. 12, which are obtained by adding all the frequency components in the respective 1/3 octave band. For example, the 1000 Hz 1/3 octave band, which is between 890 and 1125 Hz, is obtained by summing 900, 950, 1000, 1050 and 1100 Hz components of the frequency components calculated by STFT

$$\mathrm{SPL}_{1000\,\mathrm{Hz}} = 10\log_{10}\left(\sum_{i=1}^{6} 10^{\mathrm{SPL}_i/10}\right). \tag{24}$$

Fig. 12 shows that the STFT has the same temporal resolution at all frequencies; therefore the resolution obviously becomes insufficient at high frequencies.

5.4. Airbag deployment sound

The noise generated by deployment of automotive airbags can cause serious damage to auditory systems [14,15]. Fig. 13 shows a measured time-history of the airbag sound downloaded from the Army Research Lab website [14]. The instantaneous SPL of the sound reaches to nearly 6000 Pa (170 dB).

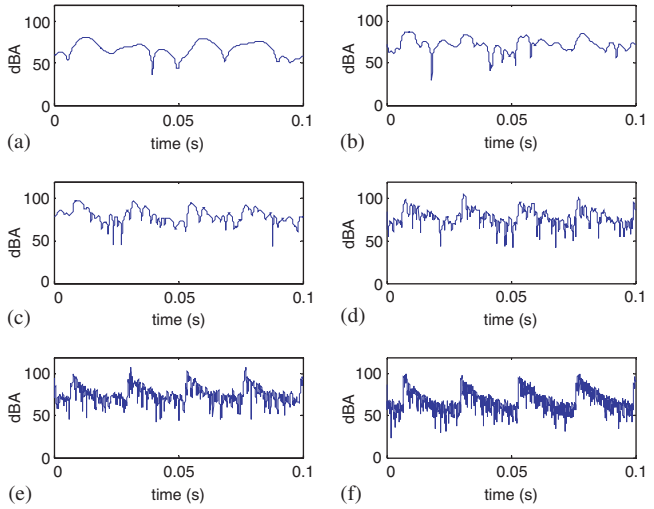

Fig. 11. 1/3 octave time histories of the impact power wrench noise obtained by AWT: (a) 500 Hz band, (b) 1000 Hz band, (c) 2000 Hz band, (d) 4000 Hz band, (e) 8000 Hz band, and (f) 16,000 Hz band.

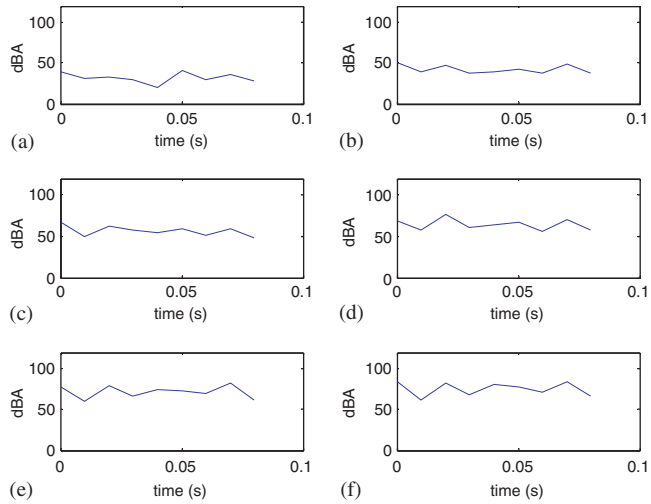

Fig. 12. 1/3 octave time histories of the impact power wrench noise obtained by STFT: (a) 500 Hz band, (b) 1000 Hz band, (c) 2000 Hz band, (d) 4000 Hz band, (e) 8000 Hz band, and (f) 16,000 Hz band.

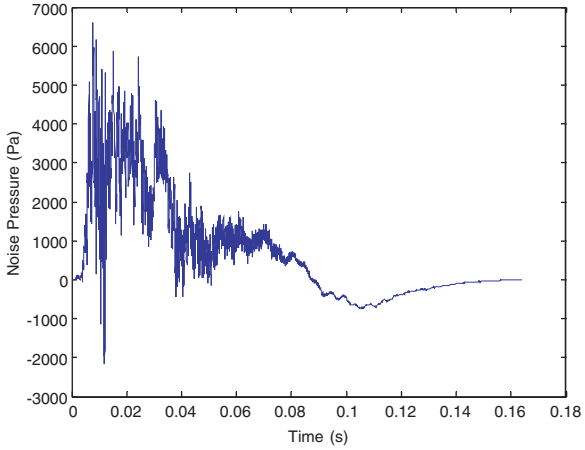

Fig. 13. Time history of the noise from deployment of an airbag.

Figs. 14 and 15 are *T–F* plots of the sound obtained from the STFT and AWT, respectively. Again, the AWT result shows much clearer, detailed information. Fig. 16 shows time histories of the 1/3 octave band SPLs at 125, 250, 500, 1000, 2000 and 4000 Hz obtained from the AWT. The 2000 Hz band shows the highest instantaneous pressure, which reaches nearly to 160 dBA. This indicates that a more detailed study will be necessary around the location in the auditory organ corresponding to this frequency. 1/3 octave time histories obtained from the STFT result are shown in Fig. 17, which again does not have sufficient temporal resolutions. Because the frequency resolution of the STFT was 50 Hz, the 1/3 octave band at 125 Hz did not include any frequency components, thus resulted in a blank plot.

6. Conclusion and discussions

Analytic wavelet transform (AWT) is advocated as a much superior alternative to the STFT for transient signal analysis in this paper. The underlying theory of the AWT is discussed in relation to the Fourier transform, which helps understanding basic properties and unique characteristics of the AWT. It is shown that

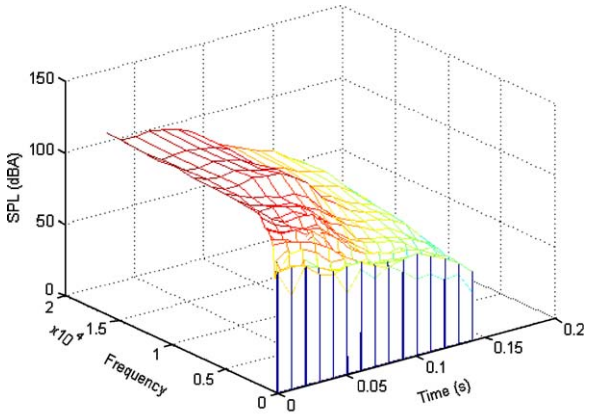

Fig. 14. Time–frequency plot of the airbag noise by STFT.

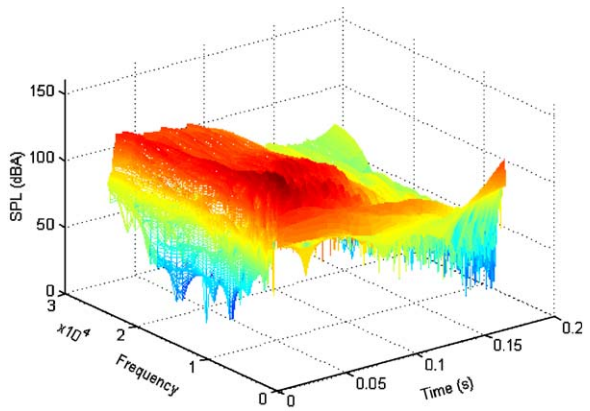

Fig. 15. Time–frequency plot of the airbag noise by AWT.

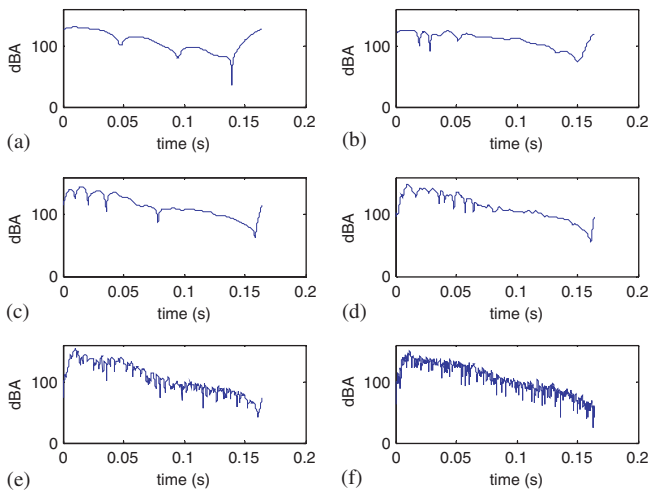

Fig. 16. 1/3 octave band SPL time histories of the airbag noise obtained by AWT: (a) 500 Hz band, (b) 1000 Hz band, (c) 2000 Hz band, (d) 4000 Hz band, (e) 8000 Hz band, and (f) 16,000 Hz band.

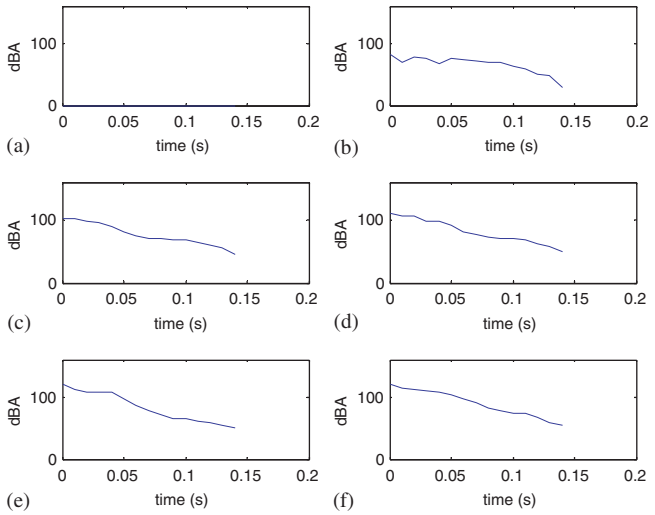

Fig. 17. 1/3 octave band SPL time histories of the airbag noise obtained by STFT: (a) 500 Hz band, (b) 1000 Hz band, (c) 2000 Hz band, (d) 4000 Hz band, (e) 8000 Hz band, and (f) 16,000 Hz band.

the AWT may be considered as a transient version of the Fourier transform because it finds both the magnitude and phase of frequency components of the signal as functions of time. Basic properties of the AWT are observed by applying it to two sets of test signals, a sine wave and a Dirac delta function, whose *T–F* representations are known in exact form.

After setting up the AWT as a transient 1/3 octave analyzer, the AWT is applied to two highly impulsive acoustic signals: an impact wrench noise and an airbag deployment noise. The AWT results are presented in the *T–F* domain in terms of the sound pressure level (SPL) in dBA. Comparison of the results with those obtained from the STFT clearly shows the main advantage of the AWT over the STFT in capturing detailed *T–F* characteristics of the signal. The transient 1/3 octave time history is introduced as a new concept, which is potentially very useful for risk assessment of impulse noise-induced hearing loss (NIHL).

With the set-up used in this work, the end users can use the AWT and interpret the result exactly in the same way as they have been doing with the STFT. End-users who have been using the STFT can use the AWT without noticing any difference while obtaining much more detailed *T–F* characteristics of the signal.

Acknowledgments

Matlab programs developed by researchers in Stanford University posted in Wavelab 802 web site [16] were used as the basis to develop the AWT program used in this work. Financial support for this work was provided by the National Institute for Occupational Safety and Health.

References

[1] S. Mallat, *A Wavelet Tour of Signal Processing*, Academic Press, San Diego, 1997.
[2] NIOSH, Preventing Occupational Hearing Loss—A Practical Guide, US Department of Health and Human Service, Centers for Disease Control and Prevention, National Institute for Occupational Safety and Health, Cincinnati, OH, DHHS (NIOSH) Publication No. 95-105, 1996.
[3] J.H. Lee, J. Kim, H.-J. Kim, Development of enhanced Wigner–Ville distribution function, *Journal of Mechanical Systems and Signal Processing* 15 (2001) 367–398.
[4] A. Grossmann, J. Morlet, Decomposition of Hardy functions into square integrable wavelets of constant shape, *SIAM Journal on Mathematical Analysis* 15 (1984) 723–736.
[5] I. Daubechies, *Ten Lectures on Wavelets*, SIAM, Philadelphia, 1992.
[6] E.O. Brigham, *The Fast Fourier Transform and Its Application*, Prentice-Hall, Upper Saddle River, 1998.

[7] *ISO-1999, Acoustics—Determination of Occupational Noise Exposure and Estimation of Noise-Induced Hearing Impairment*, second ed., Geneva, Switzerland, 1990.
[8] NIOSH, Criteria for a Recommended Standard—Occupational Noise Exposure, US Department of Health and Human Service, Centers for Disease Control and Prevention, National Institute for Occupational Safety and Health, Cincinnati, OH, DHHS (NIOSH) Publication No. 98-126, 1998.
[9] W. Passcheir-Vermeer, Measurement and rating of impulse noise in relation to noise-induced hearing loss, in: *Proceedings of the Fourth International Congress, Noise as a Public Health Problem*, Milano, Italy, 1983, pp. 143–157.
[10] W.A. Ahroon, R.P. Hamernik, R.I. Davis, Complex noise exposure: an energy analysis, *Journal of Acoustical Society of America* 93 (1993) 997–1006.
[11] M. Roberto, R.P. Hamernik, R.J. Salvi, D. Henderson, R. MilonE, Impact noise and the equal energy hypothesis, *Journal of Acoustical Society of America* 77 (1985) 1514–1520.
[12] J. Starck, E. Toppila, I. Pyykko, Impulse noise and risk criteria, *Noise and Health* 5 (2003) 63–73.
[13] P. Kulkarni, X. Zhu, J. Kim, C. Hayden, Time–frequency characteristics of high-intensity, fast transient noise from power tools by analytic wavelet transform, in: *Proceedings of the NOISECON 2004,* Baltimore, MD, 2004, pp. 306–312.
[14] G.R. Price, J.T. Kalb, Mathematical model of ear hazard from impulse noise (http://www.arl.army.mil/ARL-Directorates/HRED/AHAAH/), 2005.
[15] G.R. Price, J.T. Kalb, Auditory hazard from airbag noise exposure, *Journal of Acoustical Society of America* 106 (1999) 2629–2637.
[16] D. Donoho, M.R. Duncan, X. Huo, Wavelab 802 for MATLAB 5.x, http://www-stat.stanford.edu/~wavelab/, 2005.